SCIENCE CHINA
Technological Sciences

• Article •

June 2016 Vol.59 No.6: 867–875
doi: 10.1007/s11431-016-6061-y

Molecular dynamics simulation of single crystal Nickel nanometric machining

ZHU ZongXiao*, GONG YaDong, ZHOU YunGuang & GAO Qi

School of Mechanical Engineering & Automation, Northeastern University, Shenyang 110819, China

Received January 8, 2016; accepted March 14, 2016; published online May 16, 2016

Molecular dynamics simulation is carried out to study the nanometric machining of single crystal Nickel (Ni). Through an investigation of atomic displacement and the variation of cutting force, it is found that the latter is in accordance with the number variation of elastic displaced atoms in the workpiece. It is further found that the generation of complex stacking faults is the predominant cause of cutting force fluctuation, and the stacking faults with complex structures lead to work-hardening. The temperature of the cutting tool and workpiece is studied during the machining process. It is concluded that the selection of averaging steps has a significant influence on the system temperature distribution. Thus, the time-spatial averaging method, which has a high accuracy and consistency in temperature distribution, is proposed.

molecular dynamics simulation, cutting force, complex stacking fault, temperature distribution, time-spatial averaging method

Citation: Zhu Z X, Gong Y D, Zhou Y G, et al. Molecular dynamics simulation of single crystal Nickel nanometric machining. Sci China Tech Sci, 2016, 59: 867–875, doi: 10.1007/s11431-016-6061-y

1 Introduction

The rapid development of materials science and the increased demand for high-performance parts in modern technology result in the widespread use of single-crystal parts [1–4]. In order to provide theoretical evidence for the machining of single-crystal parts, the machining mechanism and other characteristics of single-crystal materials are well studied at the nanoscale, with consideration given to their special lattice structure [5,6]. In nanometric machining, material removal takes place in a limited region, and only several layers of atoms are removed during the process. Thus, it is difficult to observe the nanometric machining process at such a limited scale through experimental studies [7,8]. In traditional microscopic machining, the well-established continuum theory is sufficient to explain various machining phenomena which occur in continuous, isotropic, and defect-free materials. However, the essence of nanometric machining is the interaction between discrete atoms, which are governed by appropriate inter-atomic potentials. Therefore, the molecular dynamics (MD) simulation, as one of the most powerful atomic-scale simulation methods, is applied to study the detailed behavior and mechanism of materials at the atomic level.

In the late 1950s, Alder and Wainwright [9] applied the MD method in the study of statistical mechanics. Since then, this simulation method has been applied in many areas, e.g. materials science and mechanical engineering. In terms of nanometric machining, single crystal copper has been well-researched from many aspects. Since its lattice structure is the same as that of single crystal Nickel, and both of them are face-centered cubic (FCC) structures, the previous studies on single crystal copper provide great inspiration for studying the machining mechanism of single crystal Nickel.

*Corresponding author (email: zhuzongxiaoneu@163.com)

Ji et al. [10] studied the friction behavior along the tool/chip interface in nanometric machining of single crystal copper, and the results show that the normal force consistently increased when a larger negative rake angle tool was used. Lin and Huang [11] studied the influence of cutting speed on the cutting force and the strain-stress behavior of single crystal copper. Cutting force fluctuation and atomic temperature were studied by Su and Tang [12], and the simulation results showed that the different cutting velocities led to different deformation behavior in the chips. Pei et al. [13] studied the effect of inter-atomic potentials on cutting results, and found that the Morse potential resulted in larger (approximately 5%–70% larger) cutting forces than the EAM potential. Thermal effects and defects were studied by Guo and Yang [14], and they concluded that the system temperature showed as a concentric shape, and the chip had the highest temperature. Zhao et al. [15] studied the subsurface damage during nanomachining. With regard to the MD simulation related to single crystal Nickel (Ni), MD and finite element deformation model (MDFM) were combined to calculate the stress and strain of a single crystal Ni material by Lin et al. [16] during nanoscale machining. Muhammad et al. [17] studied the dynamic characteristics of nanoindentation in Ni by MD simulation.

The previous studies had tremendous value in perceiving the nanometric machining mechanism. However, there are a number of studies covering the relations between cutting force and complex stacking faults in single-crystal Ni machining. In some cases, cutting tools were considered as rigid tools with simple shapes and structures, which may greatly influence the results of nanometric machining. On the other hand, the time-averaging method is always used to study the thermal characteristics of simulated systems. However, there is an obvious energy loss caused by this method, so this thesis adopts the time-spatial averaging method to make significant improvement.

2 Simulation model and computation

2.1 The MD simulation model

The simulation model, as shown in Figure 1, consists of a single-crystal Nickel workpiece and a diamond cutting tool. The workpiece contains 152850 Ni atoms and has a size of $83a_0\times30a_0\times15a_0$ (a_0=3.52 Å) along the (1 0 0), (0 1 0), and (0 0 1) directions, respectively. The nose radius of the tool is 0.5 nm, and the rake and clearance angles are 15º and 9º, respectively. Both the workpiece and tool contain three kinds of atoms: Newton, thermostatic, and boundary atoms. Newton atoms are the main atoms used to investigate various aspects pertaining to the cutting process, as the motion of Newton atoms obeys Newton's second law. Thermostatic atoms are used to ensure heat dissipation in Newton atoms, and the temperature of the thermostatic atoms is controlled by rescaling the atom velocities every ten steps (the time step is 1 fs). Boundary atoms are fixed in order to avoid the overall movement of the workpiece during simulation. The diamond tool contains 8265 carbon atoms. At a cutting speed of 200 m/s, the tool cuts the workpiece along the (1 0 0) direction to a cutting depth of 15 Å. The periodical boundary condition is maintained along the *z*-direction, whereas the non-periodical boundary condition is applied to the *x*- and *y*-directions.

2.2 Inter-atomic potential

The potential describes the interaction between atoms, and is of great importance to the accuracy of the simulation results. In the simulation, the EAM potential is applied to describe the interaction between Ni atoms [18], which is commonly used to describe the interaction between metal atoms. The total potential is expressed by

$$E_{\text{tot}} = \frac{1}{2}\sum_{ij}\phi_{ij}(r_{ij}) + \sum_{i}F_i(\rho_i), \tag{1}$$

$$\rho_i = \sum_{j\neq i}\rho_j(r_{ij}). \tag{2}$$

In the above expression, E_{tot} represents the total potential energy; $\phi_{ij}(r_{ij})$ is the pair potential between atoms i and j which are separated by a distance r_{ij}; $F_i(\rho_i)$ is the embedded energy induced by the embedding of atom i; and ρ_i is the electron density of host atom i.

The interaction between Ni-C is described by Morse potential [19], and the expression is given by

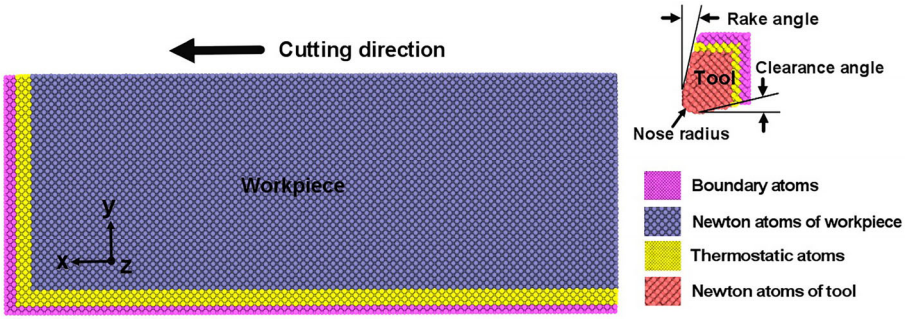

Figure 1 (Color online) MD simulation model of nanometric machining (2D representation).

$$V(r_{ij}) = D_e[\mathrm{e}^{2\alpha(r_e - r_{ij})} - 2\mathrm{e}^{\alpha(r_e - r_{ij})}], \tag{3}$$

where D_e is the cohesive energy between atoms i and j, α is the elastic modulus of the material, r_{ij} is the instantaneous distance between atoms i and j, and r_e is the equilibrium distance between atoms i and j. The parameter of Morse potential can be adopted from Lin et al. [16] as D_e=0.100 *ev*, α=2.2 Å^{-1}, r_e=2.4 Å. The C-C interaction is described by the Tersoff potential [20], which is given by

$$E = \sum_I E_i = \frac{1}{2}\sum_{i \neq j} V_{ij}, \tag{4}$$

$$\begin{cases} V_{ij} = f_C(r_{ij})[f_R(r_{ij}) + b_{ij} f_A(r_{ij})], \\ f_R(r_{ij}) = A\exp(-\lambda r_{ij}), \\ f_A(r_{ij}) = -B\exp(-\mu r_{ij}), \end{cases} \tag{5}$$

$$f_c(r_{ij}) = \begin{cases} 1, & (r_{ij} < R), \\ \dfrac{1}{2} + \dfrac{1}{2}\cos\left(\pi\dfrac{r_{ij} - R}{S - R}\right), & (R < r_{ij} < S), \\ 0, & (r_{ij} > R), \end{cases}$$

$$\begin{cases} b_{ij} = (1 + \beta_i^n \xi_{ij}^n)^{-1/(2n)}, \\ \xi_{ij} = \sum\limits_{k \neq i,j} f_c(r_{ik}) g(\theta_{ijk}), \\ g(\theta_{ijk}) = 1 + \dfrac{c^2}{d^2} - \dfrac{c^2}{d^2 + (h - \cos\theta_{ijk})^2}, \end{cases} \tag{6}$$

where E_i is the potential energy of atom I, V_{ij} is the potential energy function between atoms i and j, f_R and f_A are the repulsive and attractive interaction functions, respectively between the atoms, f_c is the cut-off distance to limit the range of potential, b_{ij} is the modulation function, r_{ij} is the distance between atoms i and j, θ_{ijk} is the angle between atoms *i-j* and *i-k*, and ξ_{ijk} is the number of bonds to atom I, with the exception of the *i-j* bond.

2.3 The method of computing temperature

In MD simulation, the temperature distributions in the workpiece and tool are investigated by converting the kinetic energy of the atoms to the thermal energy of the system. The equation is given by

$$E_{\mathrm{kin}} = \frac{1}{2}\sum_i m_i v_i^2 = \frac{3}{2}\sum_i k_B T_i = E_{\mathrm{therm}}, \tag{7}$$

where E_{kin} and E_{therm} are the kinetic energy and thermal energy of the workpiece, respectively; m_i, v_i, and T_i are the mass, instantaneous velocity, and temperature of workpiece atom i, respectively; and k_B is the Boltzmann constant. In order to obtain the true temperature of the cutting tool, one part of kinetic energy brought about by the initial cutting speed should be subtracted. The equation is given by

$$E_{\mathrm{kin}} = \frac{1}{2}\sum_i m_i (v_i - v_t)^2 = \frac{3}{2}\sum_i k_B T_i = E_{\mathrm{therm}}, \tag{8}$$

where v_t is the cutting speed of the cutting tool; E_{kin} and E_{therm} are the kinetic and thermal energy of the tool, respectively; m_i, v_i, and T_i are the mass, instantaneous velocity, and temperature of tool atom i, respectively, and k_B is the Boltzmann constant. Since the instantaneous thermodynamic value of the atoms varies, the temperature distributions of the workpiece and tool atoms are usually obtained by averaging the temperature of each atom during a certain number of time steps. In previous studies, the time averaging method was used directly in the machining process, and the selection of averaging steps is highly subjective. In addition, this method fails to accurately describe the temperature distribution of a studied system at a given moment due to the overall kinetic energy loss. In this study, the time-spatial averaging method is adopted for the system temperature distribution. The time-spatial averaging method is conducted in two steps. First, the time-averaging method with a few averaging steps is applied to ensure the accuracy of atomic temperature. Second, the average temperature of the neighboring atoms is used to express the temperature of atom i by the spatial averaging method. The workpiece is divided into grids of size $2a_0$, and the temperature of each atom within the grid can be expressed as the average temperature of the atoms within the grid.

3 Result and discussion

3.1 Cutting force and workpiece deformation

The force acting on a single atom is derived by summing the overall forces contributed by the surrounding atoms, and the cutting force is expressed by adding forces on all tool atoms. As shown in Figure 2, cutting forces change according to cutting distance. *Fx* and *Fy* denote the tangential and thrust force, respectively. Since the direction of *Fx* is opposite to the positive direction of the *x*-axis, its value is negative. Furthermore, since only several layers of atoms are removed in the machining process, it is reasonable that the magnitude of the thrust force is approximately similar to that of the tangential force, and this result is consistent with the findings of other researchers [14].

The machining process can be divided into two stages according to the degree of variation in the cutting forces. The stage at which the cutting distance is less than 8 nm is defined as the early stage of machining, and the stage at which the cutting distance more than 8 nm is defined as the stable stage of machining. As shown in Figure 2, both forces increase and vary considerably in the early stage. Then, the forces not only decrease, but also vary within a small range when machining enters the stable stage.

In detailed analysis of periods 1, 2, and 3, it is discovered that the fluctuation cycle of the two forces is the same, and the peak and valley values of the two forces appear at the same phase, as shown in Figure 2. This is because the stacking faults extend along the slip plane at an angle of 45° to the *x*- and *y*-axes, and affect both forces simultaneously. As the variation trend of the two forces is the same, it is reasonable to combine these forces to analyze the corresponding relations between material deformation and cutting forces. The combined force F is obtained by the equation:

$$\sqrt{F_x^2 + F_y^2} = F\,. \tag{9}$$

Since the displacement of each atom is a useful measure to track deformation of the workpiece atoms, the method of atomic displacement is applied. This involves computing the current displacement of each atom from its original coordinates. Then, four representative moments (a, b, c, d) are selected to analyze the relation between atomic displacement and cutting force. The total displacement of each atom is computed as

$$\sqrt{dx^2 + dy^2 + dz^2} = d(r). \tag{10}$$

There is a direct correlation between the forces acting on the atoms and the displacements of these atoms, in particular when these displacements are elastic i.e., the atomic bonds of the displaced atoms are not destroyed, and the displacements of these atoms can be recovered. The cutting force increases with an increasing number of elastic displaced atoms. This is due to the fact that each elastic displaced atoms absorbs a certain amount of energy, which is provided by the cutting tool. Thus the increase in these elastic displaced atoms leads to a sustained increase in cutting energy. In addition, the cutting force increases, and vice versa.

As shown in Figure 3, the cutting force consistently increases from time a to time b, and the number of atoms with displacements between 0.2 and 0.8 nm increases as shown in Figure 4. The cutting force fluctuates at time b, while a distinct separatrix L_1 occurs on the surface of the workpiece as shown in Figure 5(b). This indicates that dislocations are generated inside workpiece.

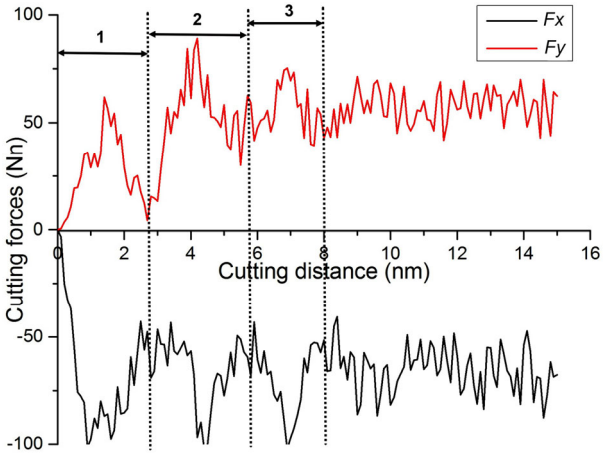

Figure 2 (Color online) Cutting forces.

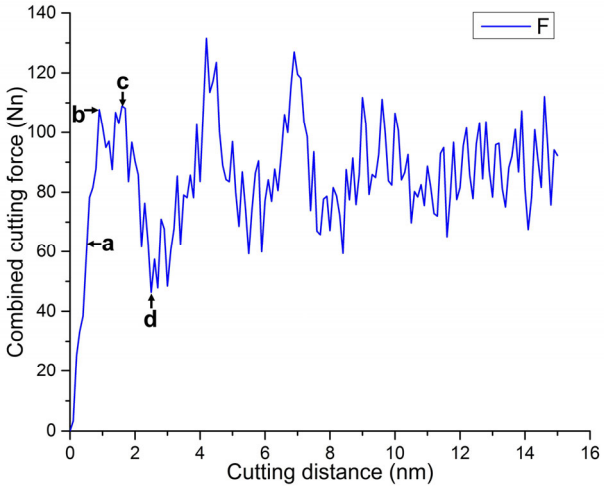

Figure 3 (Color online) Combined cutting force. The cutting distances of a, b, c and d are 0.5, 0.8, 1.6, and 2.6 nm, respectively.

The value of the cutting force increases from time b to c, as shown in Figure 3. In addition, the number of atoms with displacements between 0.2 and 1.1 nm increases, as shown in Figure 4. Three lines (L_1, L_2 and L_3) caused by different dislocations gradually extend in the workpiece in order to form the glide path to release stored energy. However, separatrix L_2 cuts off L_1 and forms a glide path until time c, as shown in Figure 5(c), so that the atoms can move along the glide path to form the chip.

As shown in Figure 3, the cutting force consistently decreases to the minimum value from time c to time d. The number of atoms with displacements between 0.2 and 1.1 nm rapidly decreases, as shown in Figure 4. This indicates that these atoms are predominantly subject to elastic dis-

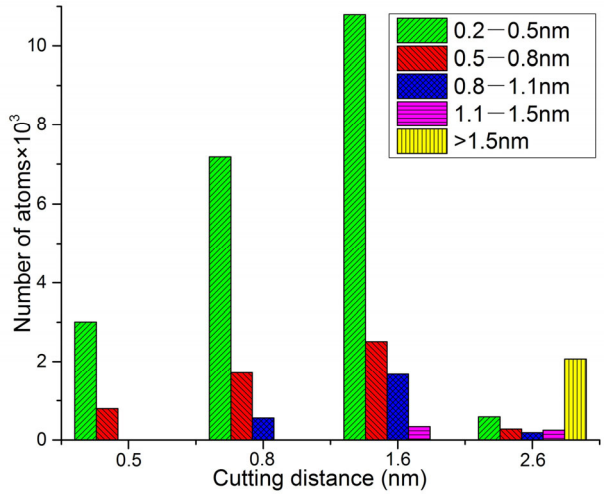

Figure 4 (Color online) The number of elastic displaced atoms at different cutting distances.

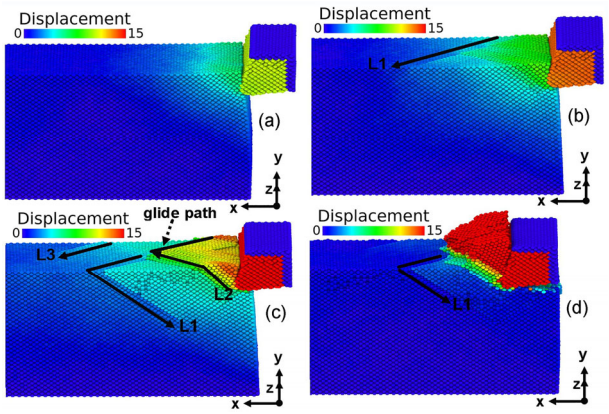

Figure 5 (Color online) Snapshot of atomic displacement at the machining moment of a, b, c and d. The cutting distance is (a) 0.5 nm, (b) 0.8 nm, (c) 1.6 nm, and (d) 2.6 nm.

placements. The elastic displacements of these atoms are recovered as a result of the formation of the glide path, while the stored energy is released and the cutting force decreases. It can be concluded that the increase or decrease in the cutting force corresponds to an increase or decrease, respectively, of the number of elastic displaced atoms. In addition, the fluctuation in the cutting force is caused by the generation and evolution of dislocations.

3.2 The defects affecting cutting force

During the process of machining simulation, it is found that the generation and disappearance of stacking faults change with the feeding of the cutting tool, and the generation of complex stacking faults is the predominant cause of the cutting force becoming larger. In order to show the defect structure clearly, in Figure 6 the perfect FCC atoms are removed; the white atoms represent dislocation and surface; the red atoms represent the HCP atoms; and two adjacent red lines represent a stacking fault.

As shown in Figure 6(a), workpiece atoms in close proximity to the tool tip produce several dislocations along the $(1\bar{1}1)$ plane, and stacking faults gradually extend on the $(1\bar{1}1)$ plane. A further stacking fault extends on the $(\bar{1}11)$ plane simultaneously, such that the dislocations and stacking faults on the $(1\bar{1}1)$ plane are blocked by the stacking fault on $(\bar{1}11)$ plane, and the dislocation block occurs in front of cutting tool. On the one hand, the dislocation block results in the proliferation of homologous dislocations and stacking faults, on the other hand, new defect 1 starts to nucleate, bypassing the obstacle stacking fault. In addition, cutting force increases with an increase in blocked dislocations, and the relevant experiments show that the dislocation density increased in the process of work-hardening.

The perfect FCC atoms, surface atoms and dislocation atoms are removed, as shown in Figure 6(b). It can be clearly observed that the stacking fault on the $(\bar{1}11)$ plane is destroyed by a series of parallel stacking faults on the $(1\bar{1}1)$ plane. Plastic deformation occurs during this process, and the cutting force suddenly decreases due to the formation of gap 3. Meanwhile, a new stacking fault 2 continues to extend in the workpiece.

As shown in Figure 6(c), the stacking fault may gradually be destroyed, which block other stacking faults from extending, and the third stacking fault 4 begins to extend on the $(\bar{1}11)$ plane. Therefore, the cutting force decreases due to the released cutting energy. It is concluded that the dislocation block is one of the causes of work-hardening.

After the dislocation block disappears, partial dislocations on the (111) and $(1\bar{1}1)$ planes result in dislocation reactions and form Lomer-Cottrell (L-C) dislocations, as shown in Figure 7(a). The (111) and $(1\bar{1}1)$ planes are represented by ABC and DBC, respectively in the Thompson tetrahedron, as shown in Figure 7(b). Partial dislocation DB resolves into Dα and αB on the DBC plane, and partial dislocation BA resolves into Bδ and δA on the ABC plane. These two processes can be expressed as

$$\frac{1}{2}[011]\longrightarrow\frac{1}{6}[121]+\frac{1}{6}[\bar{1}12],$$
$$\frac{1}{2}[\bar{1}10]\longrightarrow\frac{1}{6}[2\bar{1}\bar{1}]+\frac{1}{6}[1\bar{2}1].$$

The extended dislocations αB and Bδ generate a new dislocation αδ on the intersection of two planes. This reaction is expressed by

$$\frac{1}{6}[\bar{1}12]+\frac{1}{6}[2\bar{1}\bar{1}]\longrightarrow\frac{1}{6}[101].$$

The Burgers vector of stair-rod dislocation αδ is $\frac{1}{6}[101]$, and the glide plane of this newly formed disloca-

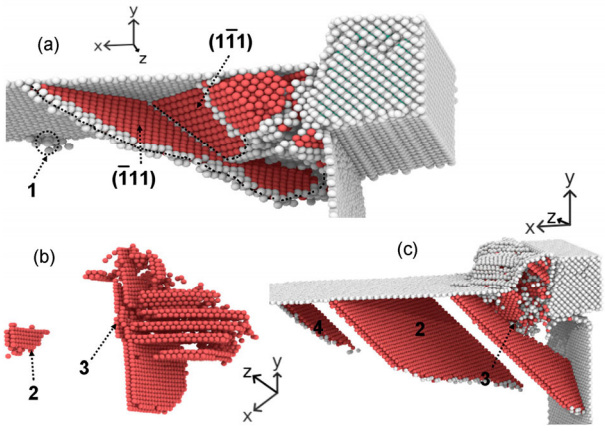

Figure 6 (Color online) Snapshots of defect evolution at different machining moments. The cutting distance is (a) 1.0 nm, (b) 1.2 nm, (c) 2.6 nm.

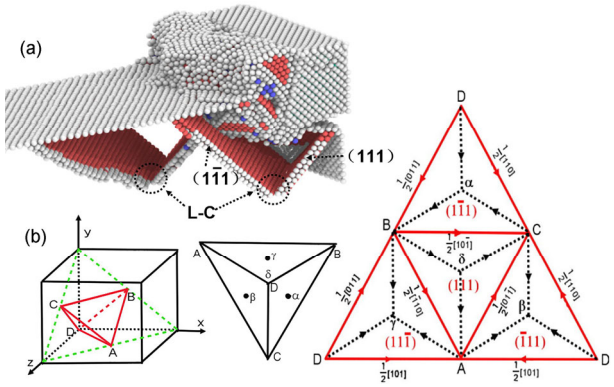

Figure 7 (Color online) (a) Snapshot of L-C dislocation at a cutting distance of 3.2 nm; (b) sketch of Thompson tetrahedron structure.

tion is (010). This vector and glide plane are not associated with the studied crystal, Thus, this newly formed dislocation can glide on neither its glide plane nor the glide plane of studied crystal. Therefore, the stair-rod dislocation αδ is an L-C dislocation. Dislocations with this structure could become a barrier to the development of other dislocations. However, this defect could be destroyed by high temperature and pressure when cutting force increases to a certain extent. Thus, the generation of this defect is one of the reasons why cutting force increases.

It is found that the cutting force becomes smaller during the stable stage of machining, and the variation range of the cutting force also becomes smaller. As shown in Figure 8, massive stacking faults are no longer generated during the stable stage of machining. This is because a high temperature and high pressure zone made up of disordered atoms is formed in the primary shear zone. The high temperature reduces the activation barrier for dislocation nucleation, which makes the dislocation easier to nucleate [14]. In addition, when a dislocation has been nucleated in primary shear zone, it does not move away immediately, but hovers around this zone [21]. Thus, many dislocations are gathered in the primary shear zone, and some of the dislocations have an impact on the stacking faults, which are easily destroyed at high temperature. Therefore, stacking faults are destroyed by other dislocations prior to the development of complex stacking faults which could cause work-hardening. Thus, the cutting force is smaller during the stable stage.

As shown in Figure 9, the number of HCP atoms increases rapidly due to the generation of complex stacking faults at the early stage I. Moreover, the increasing rate of HCP atoms maintains at a high level before the cutting distance exceeds 8 nm. This is the reason why cutting force fluctuates severely during the early stage. At the stable stage Ⅱ, the increasing rate of HCP atoms maintains a low value. This indicates that complex stacking faults are no longer generated at this stage. Cutting force also decreases due to the absence of complex stacking faults.

Since it is known that the HCP crystal has a structure with a greater planar density than that of the FCC on the

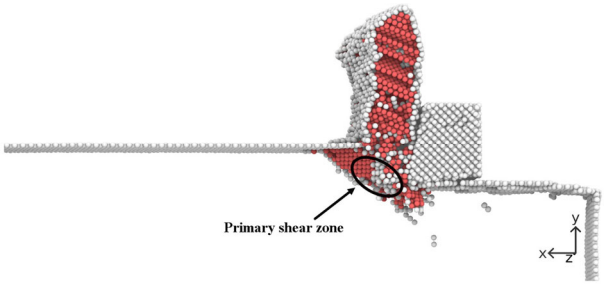

Figure 8 (Color online) Snapshot of defect evolution at a stable stage of machining.

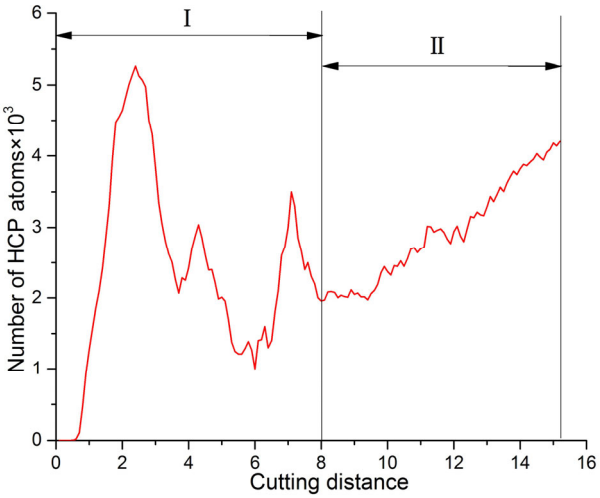

Figure 9 (Color online) Number of HCP atoms during machining.

cutting plane (010) [22], a greater cutting force is required to destroy the HCP structure. Then, complex stacking faults directly contact the front of the tool and extend into the workpiece, such that the cutting energy can be transferred into the workpiece. Therefore, stacking faults directly block the feeding of the tool. Through the above analysis, it can be concluded that stacking faults have a significant influence on cutting force, and the generation of complex stacking faults is the predominant cause of work-hardening.

3.3 Temperature

The temperature of the workpiece and tool has long been regarded as an important factor in studying nanometric machining. As shown in Figure 10, the workpiece temperature consistently increases during the machining process. Although the defect styles of the workpiece atoms are distinct at different machining times, which induces tiny fluctuations of temperature growth rate, the general temperature growth rate is not affected owing to the minor proportion of defect atoms.

The temperature increment of the workpiece is caused by extrusion and friction between the tool and workpiece. After the initial fluctuation, the cutting tool cuts into the workpiece completely. Then, the temperature of the tool gradu-

ally fluctuates around a stable value, as shown in Figure 10, which is lower than the workpiece temperature. This is because the diamond tool has a larger thermal conductivity than the workpiece. The thermostat layer atoms of the cutting tool comprise a larger proportion than that of the workpiece. Furthermore, the temperature of a single atom, or a few atoms, always fluctuates in accordance with the fluctuation of atomic kinetic energy. Thus, the small number of tool atoms is a further reason why tool temperature fluctuates severely.

The time-averaging method is always adopted when the system temperature distribution is studied. Figure 11 shows the instantaneous system kinetic energy without using any averaging method, and the system kinetic energy obtained by using different time-averaging steps during the machining process. It shows that the difference between the instantaneous and averaged kinetic energy enlarges with an increase in averaging steps. The kinetic energy with 2000 averaging steps almost reflects the real variation in instantaneous kinetic energy. However, errors become more significant as the number of averaging steps increases. Figure 12 clearly reflects the relationship between kinetic energy loss and the time-averaging steps. The curves of energy loss with different averaging steps decline during the later process of machining, as the errors between the instantaneous and averaged kinetic energy are reduced by the increase in heat dissipation during the later machining process.

The phenomenon of kinetic energy loss is predominantly because the time-averaging method is discrete. The error is generated in the system kinetic energy by this averaging method. Although the time-averaging method can successfully solve the problem of the description of single atomic temperature, this temperature lags behind the actual atomic temperature.

The disadvantages of the time-averaging method are shown in Figure 13. The high temperature zone gradually moves to the top of the chip with an increase in averaging steps.

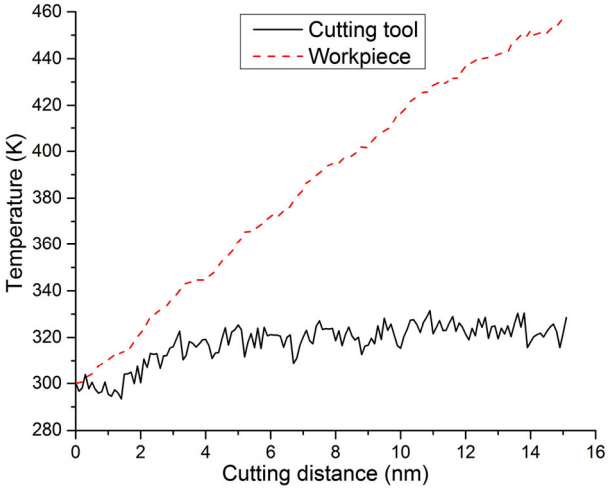

Figure 10 (Color online) Temperature variations of the tool and workpiece during machining.

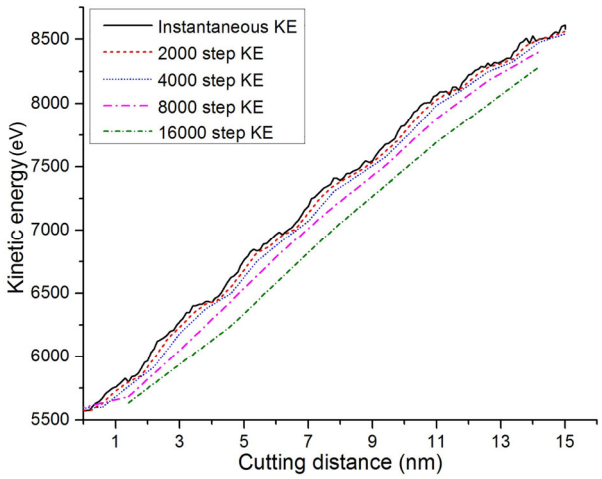

Figure 11 (Color online) Kinetic energies of different averaging steps during machining.

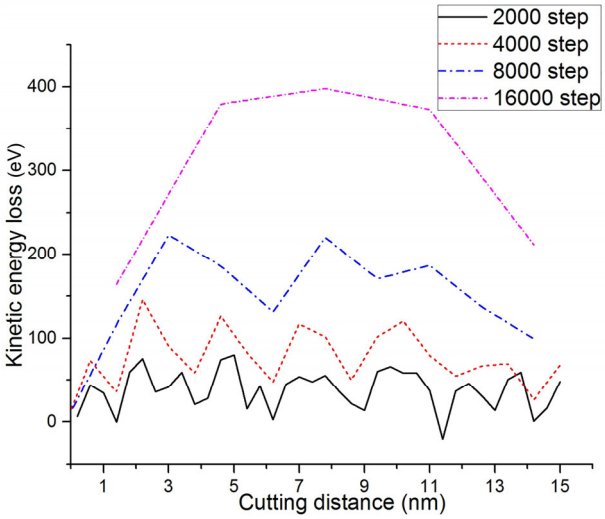

Figure 12 (Color online) Kinetic energy losses of different averaging steps during machining.

This can be seen by comparing the heights of h1, h2, h3, and h4. Meanwhile, the relatively high temperature zone of the machined surface gradually moves in the opposite direction of machining. This can be seen by comparing the lengths of s1, s2, s3, and s4. Furthermore, the time-averaging method with limited steps cannot reflect the continuity of the temperature distribution owing to the fluctuation effect of the atomic kinetic energy. This disadvantage can be mitigated by combining the time-averaging and spatial-averaging methods.

As shown in Figure 14, the temperature distributions of the workpiece and tool are obtained by the time-spatial averaging method. The temperature gradient becomes more obvious, and the continuity of temperature distribution also becomes more evident compared with that obtained by the time-averaging method.

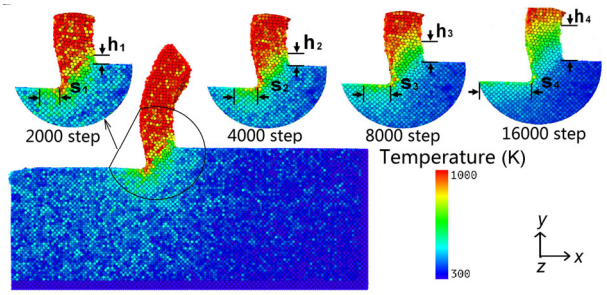

Figure 13 (Color online) Comparison of temperature distribution obtained by different averaging steps.

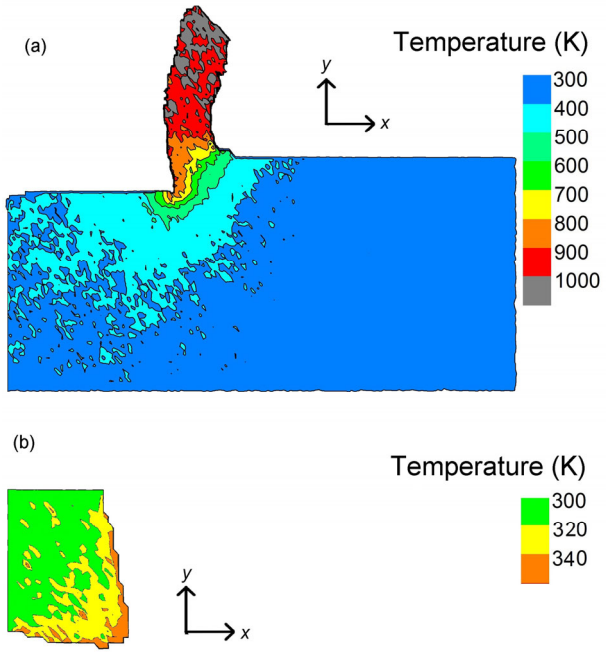

Figure 14 (Color online) Temperature distribution obtained by time-spatial averaging method.

It can be seen that the temperature distribution of the workpiece ranges from 300 to 1000 K, and the temperature gradually declines from chip to substrate. The chip has the highest temperature, because almost all of the chemical and kinetic energy of the chip atoms is transformed into heat. As shown in Figure 14(a), there exists a large temperature gradient in the shear zone. This is because this zone experiences intense extrusion and friction, and the forces acting on the atoms change dramatically.

As shown in Figure 14(b), the temperature of the cutting tool ranges from 300 to 340 K. The temperatures of the rake and flank faces are relatively higher than those of the remaining parts of the cutting tool. This is due to the direct contact with the workpiece, which is the main heat source of the diamond tool [23]. In addition, the cutting tool has a relatively lower temperature than the workpiece. On the one hand, the atomic binding energy of the cutting tool is larger than that of workpiece atoms, so it is difficult for tool atoms to transform chemical energy into heat energy. On the other hand, the cutting tool is small and has a large proportion of thermostat layer atoms. Thus, it is able to dissipate heat easily. In addition, the thermal conductivity of the diamond tool is greater than that of Nickel, and thus the generated heat can be quickly dissipated.

4 Conclusion

A molecular dynamics simulation is applied to study the nanometric machining of single crystal Nickel. The relations between cutting force, displacement of workpiece atoms, and evolution of defects are comprehensively studied. In addition, an effective method is proposed to study system temperature distribution. The following conclusions are obtained:

The variation of cutting force is in accordance with the number variation of elastic displaced atoms in the workpiece. The increase or decrease in cutting force corresponds to the increase or decrease, respectively, in the number of elastic displaced atoms.

Complex stacking faults are observed. The L-C dislocation and dislocation block are the predominant cause of work-hardening. The cutting force remains small at the stable stage of machining because of the absence of complex stacking faults.

There is a kinetic energy loss associated with the time-averaging method. Moreover, the error increases with an increase in averaging steps, and the time-spatial averaging method is proposed to analyze the temperature distributions of the workpiece and tool. This method can effectively improve the accuracy and continuity of the temperature distribution.

This work was supported by the National Natural Science Foundation of China (Grant No. 51375082).

1 Wang B B, Wang F C, Zhao Y P. Understanding formation mechanism of ZnO diatomic chain and multi-shell structure using physical mechanics. Sci China-Phys Mech Astron, 2012, 55: 1138–1146
2 Deng Y C, Quan Z H, Zhao Y H. Experimental investigations on the heat transfer characteristics of micro heat pipe array applied to flat plate solar collector. Sci China Tech Sci, 2013, 56: 1177–1185
3 Li H F, Jia R, Dou B F. Research on ultra-small textured surface of multicrystalline silicon solar cell. Sci China Tech Sci, 2013, 56: 952–956
4 Chan K T, Zhao Y P. The dispersion characteristics of the waves propagating in a spinning single-walled carbon nanotube. Sci China-Phys Mech Astron, 2011, 54: 1854–1865
5 Fatikow S, Rembold U. Microsystem Technology and Microrobotics. Berlin: Springer, 1997
6 Dong L, Subramanian A, Nelson B J. Carbon nanotubes for nanorobotics. Nano Today, 2007, 6: 12–21
7 Fang F Z, Zhang G X. An experimental study of edge radius effect on cutting single crystal silicon. Int J Adv Manuf Tech, 2003, 22: 703–707

8 Fang F Z, Wu H, Liu Y C. Modeling and experimental investigation on nanometric cutting of monocrystalline silicon. Int J Mach Tools Manu, 2005, 45: 1681–1686
9 Alder B J, Wainwright T E. Studies in molecular dynamics. I. general method. J Chem Phys, 1959, 31: 459–466
10 Ji C H, Shi J, Wang Y C, et al. A numeric investigation of friction behaviors along tool/chip interface in nanometric machining of a single crystal copper structure. Int J Adv Manuf Technol, 2013, 68: 365–374
11 Lin Z C, Huang J C. The influence of different cutting speeds on the cutting force and strain-stress behaviors of single crystal copper during nano-scale orthogonal cutting. J Mater Process Tech, 2007, 201: 477–482
12 Su H, Tang Q H. Chip formation dependence of machining velocities in nano-scale by molecular dynamics simulations. Sci China Tech Sci, 2014, 57: 2426–2433
13 Pei Q X, Lu C, Fang F Z. Nanometric cutting of copper: A molecular dynamics study. Comp Mater Sci, 2006, 37: 434–441
14 Guo Y B, Liang Y C. Atomic simulation of thermal effects and defect structures during nanomachining of copper. T Nonferrous Met Soc China, 2012, 22: 2762–2770
15 Zhao H W, Shi C L, Zhang P, et al. Research on the effects of machining-induced subsurface damages on mono-crystalline silicon via molecular dynamics simulation. Appl Surf Sci, 2012, 259: 66–71
16 Lin Z C, Huang J C, Jeng Y R, et al. 3D nano-scale cutting model for Nickel material. J Mater Process Tech, 2007, 192-193: 27–36
17 Muhammad I, Fayyaz H, Muhammad R, et al. Dynamic characteristics of nanoindentation in Ni: A molecular dynamics simulation study. Chin Phys B, 2012, 11: 116201
18 Foiles S M, Baskes M I, Daw M S. Embedded-atom-method functions for the fcc metals Cu, Ag, Au, Ni, Pd, Pt, and their alloys. Phys Rev, 1986, 33: 12–15
19 Maekawa K, Itoh A. Friction and tool wear in nano-scale machining—a molecular dynamics approach. Wear, 1995, 188: 115–122
20 Tersoff J. Modeling solid-state chemistry: Interatomic potentials for multicomponent systems. Phys Rev, 1989, 39: 8–15
21 Kitagawa H, Konishi H, Nakatani A. Study on computational modeling for materials with crystalline structure. T Jpn Soc Mech Eng A, 1991, 57: 1986–1991
22 Tong Z, Liang Y C, Yang X C, et al. Investigation on the thermal effects during nanometric cutting process while using nanoscale diamond tools. Int J Adv Manuf Technol, 2014, 74: 1709–1718
23 Norouzifard V, Hamedi M. Experimental determination of the tool-chip thermal contact conductance in machining process. Int J Mach Tools Manuf, 2014, 84: 45–57